

Estimation of Potentials of Mean Force from Nonequilibrium Pulling Simulations Using Both Minh-Adib Estimator and Weighted Histogram Analysis Method

Van A. Ngo,^{†,▽} Ilsoo Kim,^{‡,▽} Toby W. Allen,^{§,||} and Sergei Y. Noskov*,[†]

[†]Centre for Molecular Simulation, Department of Biological Sciences, University of Calgary, Alberta, AB T2N 1N4, Canada

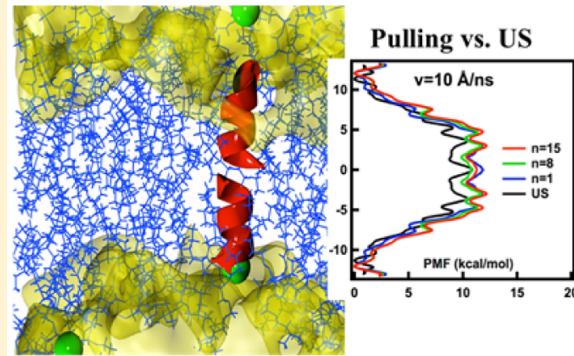
[‡]Department of Chemistry, University of Southern California, Los Angeles, California United States

[§]School of Applied Science and Health Innovations Research Institute, RMIT University, Melbourne, 3000, Australia and

^{||}Department of Chemistry, University of California, Davis California 95616, United States

Supporting Information

ABSTRACT: Nonequilibrium pulling simulations have been a useful approach for investigating a variety of physical and biological problems. The major target in the simulations is to reconstruct reliable potentials of mean force (PMFs) or unperturbed free-energy profiles for quantitatively addressing both equilibrium mechanistic properties and contributions from nonequilibrium processes. While several current nonequilibrium methods were shown to be accurate in computing free-energy profiles in systems with relatively simple dynamics, they have proved to be unsuitable in more complicated systems. To extend the applicability of nonequilibrium sampling, we demonstrate a novel method that combines Minh-Adib's bidirectional estimator with nonlinear WHAM equations to reconstruct and assess PMFs from relatively fast pulling trajectories. We test the method in a one-dimensional model system and in a system of an antibiotic gramicidin-A (gA) channel, which is considered a significant challenge for nonequilibrium sampling. We identify key parameters for efficiently performing pulling simulations to improve and ensure the convergence and accuracy of estimated PMFs. We show that a few pulling trajectories of a relatively fast pulling speed $v = 10 \text{ \AA/ns}$ can return a fair estimate of the PMF of a single potassium ion in gA.



INTRODUCTION

Jarzynski's Equality (JE)^{1,2} and Crooks' theorem (CT)^{3,4} have opened up new avenues for analyzing and investigating a number of inherently nonequilibrium processes in biological systems and quantum mechanics.^{5–7} Experiments using atomic force microscopy (AFM) and optical trap techniques^{8,9} showed that JE and CT can be used to extract equilibrium free-energy profiles from nonequilibrium pulling trajectories at various rates. Nonequilibrium pulling simulations,¹⁰ which mimic processes in AFM and optical trap techniques, have become a widespread approach for investigating the mechanical and thermodynamic properties of biological systems at detailed molecular levels. JE and CT-based approaches have been validated in many model systems governed by relatively simple free-energy profiles, which have well-separated minima and a barrier. For such systems, relatively fast pulling-speed ($\sim 1000 \text{ \AA/ns}$) simulations can be used to reconstruct the free-energy surfaces.

However, for processes or reaction coordinates involving large rearrangements in the system (conformational changes), or which are controlled by complex free-energy surfaces with many local barriers and minima, fast pulling speeds ($\geq 10 \text{ \AA/ns}$) have an impeding effect on the accuracy of JE-based and/or CT-based

reconstructions of the unbiased or unperturbed free-energy landscapes.^{11–13} For example, Kofke¹⁴ showed that a bias in data from nonequilibrium simulations indeed represents a substantial challenge for the estimation of converged free energies. Many such systems display considerable separations in the computed/measured work distribution functions used in free-energy estimations for forward and backward pulling. This is an obvious obstacle for studies of nonequilibrium processes taking place in complex systems, such as biomolecular phenomena, or, more generally, reactions in a condensed phase. Another culprit common to pulling simulations is that there appears to be no formal criterion for deciding how many pulling trajectories, in correlation with fast pulling speeds, are sufficient to obtain convergent and unbiased potential of mean forces (PMFs, or unperturbed free-energy profiles). Although Jarzynski did provide an estimate for such a number,¹⁵ its computational cost can still remain expensive, particularly for biological systems such as gA.¹¹ Therefore, a major challenge in using pulling simulations is how to accurately reconstruct unperturbed free-

Received: November 4, 2015

Published: January 22, 2016

energy profiles associated with a finite number of nonequilibrium trajectories and relatively fast pulling speeds.

Among a plethora of methods proposed to tackle this challenge, Minh-Adib's (MA) bidirectional estimator¹⁶ (also see [Methodology](#)) was able to significantly reduce bias in unperturbed free-energy profiles ($G_0(z)$) by using an optimal probability distribution of forward and backward pulling trajectories. The MA method weights forward and backward pulling trajectories in accordance with Crooks' theorem, $\frac{\rho_F(\Gamma)}{\rho_R(\Gamma)} = \exp[\beta(W - \Delta\mathcal{F})]$ where W is nonequilibrium work, $\Delta\mathcal{F}$ is a Helmholtz free energy difference between two endpoints at an inverse temperature β , and $\rho_F(\Gamma)$ and $\rho_R(\Gamma)$ are the convergent work distributions performed along trajectory Γ in the forward and backward processes, respectively. When $\rho_F(\Gamma)$ and $\rho_R(\Gamma)$ cross each other at certain pulling speeds, resulting perturbed ($\Delta\mathcal{F}(z)$) and unperturbed ($G_0(z)$) free-energy profiles can be, in principle, faithfully reconstructed.

In a one-dimensional model system, Minh and Adib showed that the method is more reliable and less expensive when using CT rather than JE, while there is apparently no criterion to assess the quality of PMFs computed from JE. Hummer and Szabo (HS)¹⁷ expanded it to a so-called quasi-harmonic approximation, which is the second-order integration expansion of the Hubbard–Stratonovich transformation between a perturbed free-energy profile ($\mathcal{F}(z)$) and $G_0(z)$ along the reaction coordinate z . Hummer and Szabo showed that an accurate estimate for $G_0(z)$ from a second-order transformation can be achieved in systems like DNA or RNA folding and unfolding processes, whose free-energy landscapes have only one bistable switch. The performance of the method for more complex processes featuring multiple stable minima and/or barriers of significantly different heights, which hinder the crossing of $\rho_F(\Gamma)$ and $\rho_R(\Gamma)$,^{14,18} has yet to be established.

While there is little doubt that nonequilibrium sampling data contain relevant information about unperturbed $G_0(z)$, retrieving it may require an additional postprocessing step. A possible treatment can be related to well-established postprocessing algorithms that already exist in the field. One of the earliest attempts was made by Gullingsrud et al.¹⁹ The authors proposed a postprocessing scheme to reconstruct $G_0(z)$ from non-equilibrium pulling trajectories by applying the weighted histogram analysis method (WHAM) equations, which are usually used to minimize the errors associated with computations of unperturbed free energies from equilibrium sampling techniques, such as umbrella sampling (US) or thermodynamics integration (TI).^{20–22} In essence, pulling trajectories can be dissected into intervals identical to lambda-windows of the umbrella sampling, and then data in the windows can be analyzed and unbiased with nonlinear-coupled WHAM equations. Gullingsrud et al., however, showed in simple model systems having sinusoidal and Gaussian-like PMF profiles that WHAM equations sometimes fail to recover accurate $G_0(z)$ from trajectories of pulling speeds $v = 1$ and 10 Å/ns. The failure was thought to be (1) the nonzero irreversible work in one-direction nonequilibrium pulling data, which are not properly removed to be used in the WHAM equations, and (2) the lack of careful sampling at steep transition points. Thus, an apparent conclusion at the time was that the WHAM equations do help remove bias, but might not be always reliable for obtaining $G_0(z)$ from nonequilibrium pulling trajectories.

As discussed above, the MA estimator can, in principle, rigorously remove bias or nonzero irreversible work in

nonequilibrium pulling data to recover $G_0(z)$, but it was not combined with the WHAM equations to assess whether any bias remains, particularly in the cases of small trajectory numbers. This causes us to ask: is it possible to better use the MA estimator and WHAM equations to analyze the unbiased or biased probability of a point in phase-space explored by a relatively fast steering potential in pulling simulations, in which $\rho_F(\Gamma)$ and $\rho_R(\Gamma)$ might not clearly cross each other? Answers to this questions will address how fast pulling speeds should be and how many pulling trajectories can be considered as sufficient for a level of accuracy, that is, bias in PMFs is minimized; thus multiple times of more trajectories would not have any significant effects.

In this paper, we will demonstrate a novel method that combines the MA bidirectional estimator with nonlinear WHAM equations to compute reliable $G_0(z)$, even in the case that $\rho_F(\Gamma)$ and $\rho_R(\Gamma)$ do not cross each other, given a small number of relatively fast pulling trajectories. The MA estimator is implemented to optimally use pulling trajectories, and the WHAM equations are solved to ensure the convergence of $G_0(z)$ from the pulling data. This paper is organized as follows: in [Methodology](#), we present the formalisms of the MA estimator and WHAM equations; then, we examine the performance of the method in a one-dimensional system ([section 1](#)) and in a system of a gramicidin A (gA) channel ([section 2](#)). In the model system, we study primarily how pulling speeds affect forward and backward work distribution functions $\rho_F(\Gamma)$ and $\rho_R(\Gamma)$, that is, the performance of the MA estimator and WHAM equations. In both systems, we identify key parameters that can return an optimal estimate of $G_0(z)$ from the pulling trajectories.

METHODOLOGY

Minh-Adib's (MA) Bidirectional Estimator. The MA estimator is based on the Crooks' fluctuation theorem^{3,4} to appropriately weigh the forward and backward pulling trajectories to reconstruct $G_0(z)$. The detailed derivation of this estimator was reported in ref 16, here we describe only the equations, which are implemented in our technique with similar notations used in ref 17. For simplicity, we present them for a one-dimensional reaction coordinate. The generalization for multidimensional reaction coordinates is straightforward.²³

Suppose there are n_f forward and n_r backward (or reverse) trajectories from pulling simulations. To perform a forward pulling simulation, a harmonic potential $V_f(z;t) = k(z - z_A - vt^2)/2$ is applied to a particle for driving the system from state A (z_A) to state B (z_B) along a one-dimensional reaction pathway, $L = z_B - z_A$, of coordinate z from time $t = 0$ to τ . To perform a backward pulling simulation, a harmonic potential $V_r(z;t) = k(z - z_B + vt)^2/2$ is used for the reverse transition from time $t = 0$ to τ . Work is computed as $W_f(z) = \int_{z_A}^z F(s_f) ds_f$ and $W_r(z) = \int_{z_B}^z F(s_r) ds_r$ for forward and backward processes, respectively, where $F(s) = k(s - z)$ with $s_f = z_A + vt$ and $s_r = z_B - vt$ for forward and backward trajectories, respectively. The perturbed free-energy

$$\mathcal{F}(z) = -\beta^{-1} \ln \int \exp(-\beta[H_0(\xi) + k(z - \xi)^2/2]) d\xi$$

with β being the inverse temperature and $H_0(\xi)$ being the unperturbed Hamiltonian of the system, can be computed from the MA bidirectional estimator,

$$\begin{aligned} e^{-\beta(\mathcal{F}(z) - \mathcal{F}(z_A))} &= \left\langle \frac{n_f e^{-\beta W_f(z)}}{n_f + n_r e^{-\beta[W_f(z_B) - \Delta\mathcal{F}]}} \right\rangle_f \\ &+ \left\langle \frac{n_r e^{-\beta[W_f(z) + \Delta\mathcal{F}]}}{n_r + n_f e^{-\beta[W_f(z_A) + \Delta\mathcal{F}]}} \right\rangle_r \end{aligned} \quad (1)$$

where $\langle \dots \rangle$ denotes the average over trajectories and $\Delta\mathcal{F} = \mathcal{F}(z_B) - \mathcal{F}(z_A)$ is estimated from the Bennett acceptance ratio (BAR),²⁴

$$\left\langle \frac{1}{n_r + n_f e^{\beta[W_f(z_B) - \Delta\mathcal{F}]}} \right\rangle_f = \left\langle \frac{1}{n_f + n_r e^{\beta[W_f(z_A) + \Delta\mathcal{F}]}} \right\rangle_r \quad (2)$$

Using $\mathcal{F}(s_f = z_A + vt)$, that is, the unperturbed free-energy profile (usually called PMF),

$$\begin{aligned} G_0(z) &= -\beta^{-1} \ln \int \delta(z - \xi) \exp[-\beta H_0(\xi)] d\xi \\ &= -\beta^{-1} \ln p_0(z) \end{aligned}$$

along the reaction pathway is computed as

$$\begin{aligned} e^{-\beta G_0(z)} &= p_0(z) \\ &= \frac{\sum_t \left[\left\langle \frac{n_f \delta(z - z_t) e^{-\beta W_f(z_t)}}{n_f + n_r e^{-\beta[W_f(z_B) - \Delta\mathcal{F}]}} \right\rangle_f + \left\langle \frac{n_r \delta(z - z_t) e^{-\beta[W_f(z_t) + \Delta\mathcal{F}]}}{n_r + n_f e^{-\beta[W_f(z_A) + \Delta\mathcal{F}]}} \right\rangle_r \right] e^{\beta \Delta\mathcal{F}(s_f)}}{\sum_t e^{-\beta[V_f(z_t; t) - \Delta\mathcal{F}(s_f)]}} \end{aligned} \quad (3)$$

where $\Delta\mathcal{F}(s_f) = \mathcal{F}(s_f = z_A + vt) - \mathcal{F}(z_A)$, $p_0(z)$ is the equilibrium probability distribution function, and $\delta(\xi)$ is the Dirac delta function.

To compute $G_0(z)$ from the expression with the Dirac delta function, one can construct histograms for evaluating the averages in eq 3. Let us denote δt as the simulation time step; thus, $N = \tau/\delta t$ is the number of steps, and the number of values of $s_f = z_A + vt$ for $t \in [0: \tau]$ is equal to $N + 1$. Let us divide the reaction pathway into $Q = Q_{\max} - Q_{\min}$ bins, with ϵ being the bin width; thus, $z = z_A + i\epsilon$, where $i \in [Q_{\min}: Q_{\max}]$. Then, $\delta(z - z_i)$ is approximated to be 1 if $|z_A + ie - z_i| \leq \epsilon/2$ or zero otherwise. We define $M(i)$ as the total count in the i th bin, summed over all forward and backward pulling trajectories. $M(i)$ will be used for WHAM. We will show that the use of only the MA estimator is not sufficient to optimally remove the bias in a finite number of relatively fast pulling trajectories (see below section 2.1), and that the WHAM equations do improve the accuracy of $G_0(z)$.

Coupled Nonlinear WHAM Equations. Note that eq 3 is sometimes regarded as a WHAM technique for the analysis of pulling data^{16,17,25} because of the above histogram-construction procedure and the presence of exponentially weighting functions. However, it was never combined with coupled nonlinear WHAM equations as shown below.

Let us consider a forward pulling trajectory in which each time step j from 0 to N is considered as a “simulation” of sampling z with the biasing potential $V_f(z; t) = k(z - z_A - vj\delta t)^2/2$. Thus, one can combine n_f values of z from n_f forward pulling trajectories into the j th “simulation”. This can similarly be performed for the backward pulling trajectories to combine n_r values of z into the “simulation” represented by the same biasing potential $V_r(z; t) = V_f(z; \tau - t)$. Given that $M(i)$ are measured in Q bins (now called windows) and that each window contains data, whose j th simulation (the same type of simulations defined by WHAM) is

precisely sampled $N_j = n_f + n_r$ times, one can construct the same likelihood probability function derived in WHAM,^{20,21} namely,

$$A(p_1, \dots, p_Q) = -\sum_{j=0}^N N_j \ln f_j - \sum_{i=Q_{\min}}^{Q_{\max}} M(i) \ln p_i \quad (4)$$

where p_i is initially equal to $\rho_0(z_A + ie)$ and $f(j)$ is the reciprocal of the partition function of simulation j , given by

$$f(j) = \frac{1}{\sum_i c(j, i) p_i} \quad (5)$$

where

$$c(j, i) = \exp \left(-\beta k \frac{\left[v\delta t \left(\frac{iN}{Q} - j \right) \right]^2}{2} \right)$$

Use of the initial values of p_i estimated from the MA estimator is the major difference from the approach by Gullingsrud et al.,¹⁹ which compute p_i by simply reweighting the biasing probability in only one-direction pulling simulations according to the umbrella sampling method. This approach, however, entails major difficulties to properly remove nonzero irreversible (or dissipated) work and sample critical points in phase space. Our proposed technique can overcome the difficulties by having dissipated work optimally removed by the MA estimator and incorporating both forward and backward pulling trajectories, which can enhance the sampling of critical points in phase space.

Note that the derivation of $A(p_1, \dots, p_Q)$ generally does not depend on the initial states, in which the data in the j th simulation are sampled; that is, data in the j th simulation can be sampled via pulling from a distant initial state. Therefore, an optimized value of $A(p_1, \dots, p_Q)$ allows for an optimal estimate of $G_0(z)$ based on the sets of initial p_i and $M(i)$. Of course, the quality of the initial p_i and $M(i)$ depends on pulling speeds and how many pulling trajectories are available, similarly to the requirements for umbrella sampling data in terms of window numbers and equilibration times. $M(i)$ may also depend on the strength of force constants (k), which affect distributions of data in Q bins or windows. For example, if k is weak, then at fast pulling speeds, some of $M(i)$ are simply zero; thus, the resulting $G_0(z)$ is likely to be compromised.

Taking the derivative of $A(p_1, \dots, p_Q)$ with respect to p_i gives us

$$\frac{\partial A}{\partial p_i} = \frac{M(i)}{(n_f + n_r) \sum_j f(j) c(j, i)} \quad (6)$$

which, with eq 5, formulates the coupled WHAM equations that minimize $A(p_1, \dots, p_Q)$. It can be observed from eq 6 that if $M(i)$ are zero in some relevant bins, eq 6 is unable to recover p_i for relevant states. Large values of k and slow pulling speeds v are crucial to have well-defined relevant states ($M(i) \neq 0$ and p_i is finite) between the two end states so accurate PMFs can be obtained.

Once all p_i are iteratively solved via eqs 5 and 6 within an accuracy tolerance, the uncertainty of $G_0(z_A + ie) - \beta^{-1} \ln p_i$ is estimated by

$$\sigma_{WHAM} = \sqrt{\frac{Q}{n_f + n_r} k_B T k \epsilon^2} \approx \sqrt{\frac{z_B - z_A}{n_f + n_r} k_B T k \epsilon} \quad (7)$$

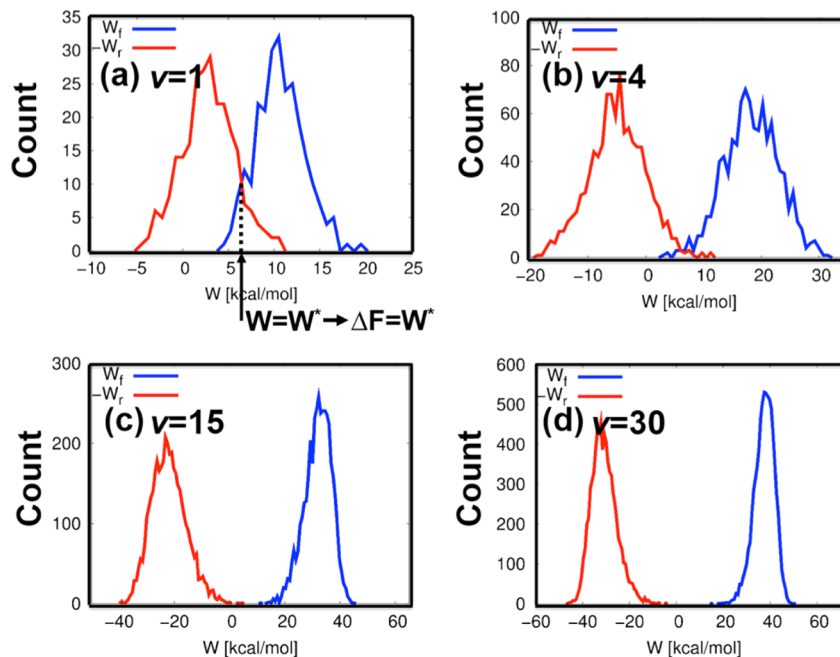


Figure 1. Forward (W_f) and backward (W_r) work histograms from nonequilibrium pulling simulations with $k = 15k_B T/\text{\AA}^2$ for the one-dimension model system. The numbers of trajectories with different pulling speeds ($v = 1, 4, 15$, and $30 \text{ \AA}/\text{ps}$) are (a) 250, (b) 1000, (c) 4000, and (d) 7500.

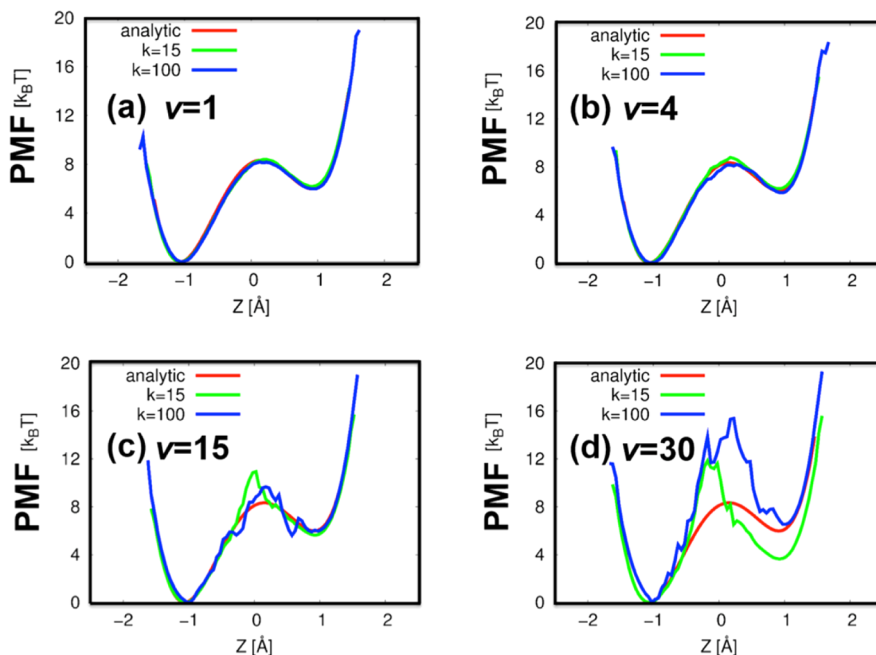


Figure 2. Unperturbed free-energy profiles or PMFs $G_0(z)$ computed by the MA estimator for the one-dimensional model system from the work distributions shown in Figure 1, and also with $k = 30k_B T/\text{\AA}^2$.

Another possible error is due to the step of combining the MA bidirectional estimator with the WHAM equations. For $Q > N$, σ_{WHAM} is the only uncertainty of the method. For $Q < N$, the histogram method might give rise to another uncertainty due to putting data z_t on a trajectory with $t \in [t_{i-1/2}:t_{i+1/2}]$ into the i th bin, where $t_{i\mp 1/2} = (\varepsilon/v)(i \mp 1/2)$. It is trivial to see that if the time interval (or bin width) is too large, the histogram will completely fail because those data belong to different perturbed free energies $\mathcal{F}(z_A + vt)$. The histogram method only works if the values of $\mathcal{F}(z_A + vt)$ in the time interval are slightly different. We found

that for reasonably small bin widths, this error has a relatively small impact on the estimated $G_0(z)$ (see below).

Systems for Testing: Model System and Gramicidin-A Imbedded in Lipid Bilayer. *1. One-Dimensional Model System.* Brownian dynamics (BD) of a one-dimensional system with a pulling harmonic potential, $u(z,t) = k/2(z - z_{A,B} \mp vt)^2$, were simulated with the model Hamiltonian, $V_0(z) = 5z^4 - 10z^2 + 3z$, as used by Minh and Adib,¹⁶ to demonstrate the performance of the only MA estimator (not with WHAM equations). Initial configurations were sampled

from the Boltzmann distribution with the potential $V_0(z) + u(z,0)$ and propagated by solving BD using the Euler algorithm,

$$z(z + \Delta t) = z(t) + \beta DF(z, t)\Delta t + \sqrt{2D\Delta t}\delta_{G(t)} \quad (8)$$

where $F(z,t) = -\partial V_0/\partial z - k(z - z_{A,B} \mp vt)$, $\beta = 1/(k_B T)$, $D = 1.0 \text{ \AA}^2/\text{ps}$ is the diffusion constant, $\Delta t = 0.001 \text{ (ps)}$ is the time step, and $\delta_{G(t)}$ is a random number sampled from the Gaussian distribution with zero mean and unit variance. Work is computed as follows:

$$W(t + \Delta t) = W(t) + u(z(t), t + \Delta t) - u(z(t), t)$$

The BD forward and backward simulations, with force constants of $k = 15$ and $100 k_B T/\text{\AA}^2$, were carried out at four pulling speeds: $v = 1, 4, 15$, and $30 \text{ \AA}/\text{ps}$, from $z = z_A = -1.5$ to $z = z_B = -1.5 \text{ \AA}$ with 250, 1000, 4000, and 7500 trajectories, respectively. These trajectories produce the same amount of data for testing the efficiency and accuracy of the MA estimator and the proposed method.

In addition to the Bennett Acceptance Ratio (BAR), that is, eq 2, three different free-energy estimators were also used to evaluate the perturbed free energy difference, $\Delta\mathcal{F} = \mathcal{F}(z_B) - \mathcal{F}(z_A)$. The first free-energy estimator is Crooks' theorem,⁴ which is a generalized expression extending the Bennett overlapping histogram (BOH),²⁶

$$\frac{\rho_F(W_{\text{diss}})}{\rho_R(-W_{\text{diss}})} = \exp(\beta W_{\text{diss}}) \quad (9)$$

where $W_{\text{diss}} = W - \Delta\mathcal{F}$ is an amount of dissipated work induced by a steering or pulling potential. The second free-energy estimator is a second-order cumulant expansion, derived by Hummer and Szabo:²⁷

$$\Delta\mathcal{F} \approx (\langle W_f \rangle + \langle -W_r \rangle)/2 - \beta[\text{var}(W_f) - \text{var}(W_r)]/12 \quad (10)$$

where W_f and W_r represent forward and backward work, respectively. The third free-energy estimator is a first-order cumulant expansion, $\Delta\mathcal{F} \approx (\langle W_f \rangle + \langle -W_r \rangle)/2$, which can be derived by requiring the symmetry of the average forward and backward dissipated works, i.e., $\langle W_f \rangle - \Delta\mathcal{F} = \langle W_f \rangle + \Delta\mathcal{F}$.²⁸

Figures 1 and 2 show forward/backward work histograms and the corresponding PMFs $G_0(z)$ computed by the MA estimator (called MA PMFs). For relatively slow pulling protocols ($v = 1$ and $4 \text{ \AA}/\text{ps}$ at $k = 15 k_B T/\text{\AA}^2$), which yield significant overlaps between the work distributions (Figure 1a,b) and small dissipated work ($W_{\text{diss}} = W_f - \Delta\mathcal{F} \approx \langle W_r \rangle + \Delta\mathcal{F} \approx 0$), Table 1 shows that all of the estimators, including the first-order

Table 1. Perturbed free energy difference $\Delta\mathcal{F} = \mathcal{F}(z_B) - \mathcal{F}(z_A)$ (in $k_B T$) at Different Pulling Speeds via Various Free Energy Estimators with a Force Constant $k = 15 k_B T/\text{\AA}^2$

$k = 15$	BAR	Crooks' Theorem (or BOH)	2nd cumulant expansion	1st cumulant expansion (LRA)
$v = 1$	6.62 ± 0.06	6.74 ± 0.09	6.61 ± 0.06	6.60 ± 0.04
$v = 4$	6.66 ± 0.08	6.75 ± 0.12	6.72 ± 0.04	6.65 ± 0.05
$v = 15$	6.46 ± 0.50	n/a (no overlap)	6.30 ± 0.04	4.90 ± 0.04
$v = 30$	2.97 ± 0.60	n/a (no overlap)	4.32 ± 0.02	3.32 ± 0.01

^aThe exact value is $6.63 k_B T$. The means and standard errors were obtained from five independent simulations for each pulling speed.

cumulant expansion, reproduce accurate numerical results in comparison with the exact perturbed free-energy difference of $6.63 k_B T$, which is computed by integrating

$$\mathcal{F}(z) = -\beta^{-1} \ln \int \exp(-\beta[V_0(\xi) + k(z - \xi)^2/2]) d\xi$$

At these pulling speeds, the MA PMFs are accurate (Figure 2a,b). However, that is not the case for the fastest pulling speed of $30 \text{ \AA}/\text{ps}$, which induces large dissipated work, $W_{\text{diss}} \gg 1$, with the two work distributions being separated by as much as $20 k_B T$ (Figure 1d). At this pulling speed, all of the free energy estimators produce inaccurate PMFs (Figure 2d) and wrong $\Delta\mathcal{F}$ (Table 1). For the pulling speed of $15 \text{ \AA}/\text{ps}$, even though the work histograms do not overlap (Figure 1c), both BAR and the second-order cumulant yield reasonably accurate values of $\Delta\mathcal{F}$ between two wells, which are smaller than the exact value ($6.63 k_B T$) by approximately 2.5–5%, while the first-order cumulant expansion fails to yield an accurate result. Figure 2c shows that their PMFs noticeably deviate from the analytic PMF near the barrier ($z = 0$). Table 2 shows that increasing the force

Table 2. Perturbed Free Energy Difference $\Delta\mathcal{F} = \mathcal{F}(z_B) - \mathcal{F}(z_A)$ (in $k_B T$) at Different Pulling Speeds via Various Free Energy Estimators with a Force Constant $k = 100 k_B T/\text{\AA}^2$. The exact value is $7.87 k_B T$

$k = 100$	BAR	Crooks' Theorem (BOH)	2nd cumulant expansion	1st cumulant expansion (LRA)
$v = 4$	7.75 ± 0.05	7.70 ± 0.06	7.77 ± 0.05	7.82 ± 0.04
$v = 15$	8.18 ± 0.32	n/a (no overlap)	7.71 ± 0.04	7.82 ± 0.03
$v = 30$	8.82 ± 0.83	n/a (no overlap)	8.05 ± 0.11	7.78 ± 0.05

constant to $100 k_B T/\text{\AA}^2$ can improve the values of estimated $\Delta\mathcal{F}$, which are less than 12% (at $v = 30 \text{ \AA}/\text{ps}$, using BAR) of differences from the exact value ($7.87 k_B T$) by all of the estimators at all of the pulling speeds. However, such an improvement of estimating $\Delta\mathcal{F}$ does not imply the clean agreement between the MA PMFs and the exact ones (Figure 2c,d), in which the values of the PMFs near the barrier ($z = 0$) remain poorly recovered at relatively fast pulling speeds ($v = 15$ and $30 \text{ \AA}/\text{ps}$). This supports the conclusion that for forward and backward work distribution functions that do not cross each other, given a small number of relatively fast pulling trajectories, it is not possible to faithfully reconstruct entire PMFs.

To improve the accuracy of the PMF reconstruction from the pulling trajectories, we dissect the pulling data and solve the WHAM equations with a convergence tolerance equal to 10^{-7} kcal/mol (see Methodology). Figure 3 shows the PMFs computed by the MA estimator and the proposed method (called MA+WHAM PMFs). First of all, the use of WHAM equations recovers the analytic PMF at $v = 4 \text{ \AA}/\text{ps}$ and $k = 100 k_B T/\text{\AA}^2$, indicating that it performs well at this pulling protocol. However, Figure 4 shows at the same pulling speed $v = 4 \text{ \AA}/\text{ps}$ that the WHAM equations can underestimate the PMF $G_0(z)$ if using $k = 15 k_B T/\text{\AA}^2$. This underestimation illustrates a point discussed in the Methodology in which strong force constants distribute data over Q bins less abruptly than soft force constants, thus recovering more accurate PMFs. Figure 3b shows that the PMFs computed by our method also depend on pulling speeds as well but are less severe than the MA estimator (see Figures 2c,d versus 3b). Specifically, at a pulling speed of $15 \text{ \AA}/\text{ps}$ and $k = 100$

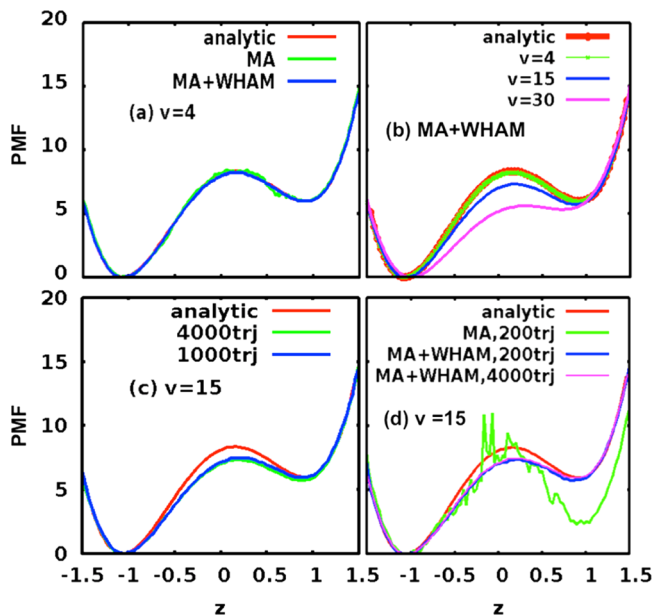


Figure 3. (a) Potential of mean force (PMF) $G_0(z)$ computed by the MA estimator and the proposed method (MA+WHAM) from 1000 trajectories with a pulling speed $v = 4 \text{ \AA}/\text{ps}$. (b) MA+WHAM PMFs at different pulling speeds. (c) MA+WHAM PMFs $v = 15 \text{ \AA}/\text{ps}$ with different numbers of trajectories. (d) PMFs computed by the MA estimator and the method from different numbers of pulling trajectories. The units for PMF and z are $k_B T$ and \AA , respectively. Force constant $k = 100k_B T/\text{\AA}^2$ is used for pulling. The bins used for the WHAM equations in this benchmark are from Q_{\min} to Q_{\max} .

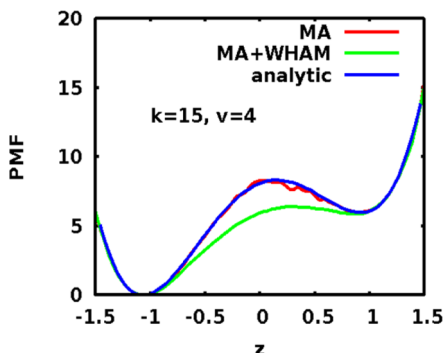


Figure 4. Potential of mean force (PMF) $G_0(z)$ computed by the MA estimator and our proposed method (MA+WHAM) from 1000 trajectories with a pulling speed $v = 4 \text{ \AA}/\text{ps}$ and $k = 15k_B T/\text{\AA}^2$. The bins used for the WHAM equations in this benchmark are from Q_{\min} to Q_{\max} . The units for PMF and z are $k_B T$ and \AA , respectively.

$k_B T/\text{\AA}^2$, both the MA and MA+WHAM PMFs noticeably deviate from the analytic PMF, particularly at $z = 0$; however, the MA+WHAM PMFs are much smoother and less noisy than the MA PMFs (Figures 2c versus 3c). The MA+WHAM PMFs have a lower barrier, at most 0.8–0.9 (~10%), than the analytic one. For the pulling speed of 30 $\text{\AA}/\text{ps}$, the reconstruction via the WHAM equations is poor because it strongly underestimates the PMF. This suggests that for very fast pulling speeds, it is likely impossible to recover accurate and unbiased PMFs from a finite number of pulling trajectories.

Figure 3 panels c and d show that our method is much more efficient in recovering convergent PMFs than the MA estimator itself for number of pulling trajectories as small as 200, when accepting an uncertainty of 10%. Additionally, five times of 200

trajectories essentially does not change the MA+WHAM PMFs, suggesting that more trajectories do not improve the optimized likelihood probability function (eq 4). This perhaps can serve as a criterion to not perform more pulling trajectories (e.g., 1000 trajectories), which may not drastically improve phase-space statistics. To this end, these results suggest that relatively slow pulling speeds and strong force constants are favorable for recovering a reliable $G_0(z)$ from only a finite number of forward and backward trajectories.

2. Gramicidin A (gA). We chose gA to examine our method and compare directly with the results obtained from umbrella sampling (US) because gA is very well studied experimentally and computationally.^{29–33} Gramicidin A, which is an antibiotic and able to conduct K^+ more favorably than Na^+ ,³⁴ has been shown to present a significant challenge for reconstructing PMFs from pulling simulations in comparison with US.¹¹ We followed the method of construction of the gA channel in a lipid bilayer (see Figure 5) as used in ref 32. The dimensions of the system are

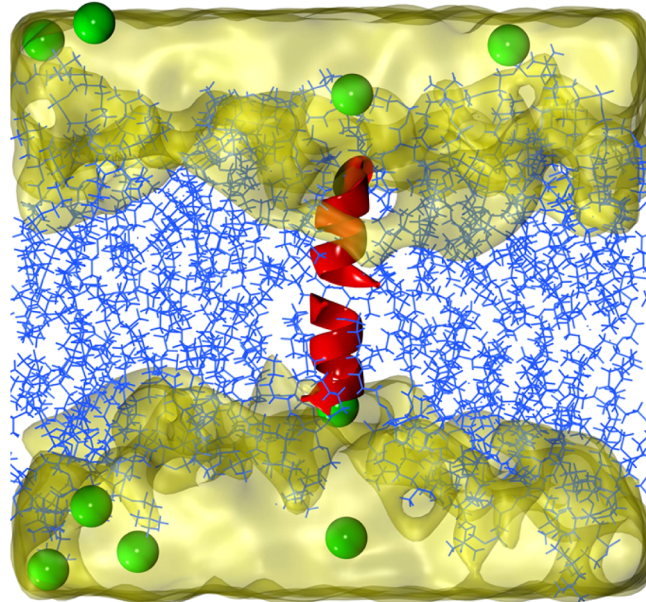


Figure 5. System of gA (red) embedded in lipid bilayer (blue). Water layers are in yellow. Green spheres are potassium ions (chloride ions not shown).

$66.7 \times 51.4 \times 60.6 \text{ \AA}^3$. The system was equilibrated with CHARMM for umbrella sampling using the C27 force field without CMAP parameters.^{35–37} To prevent the protein from drifting in the xy -plane, a cylindrical constraint of 5 kcal/mol/ \AA^2 was applied to the center of mass of gA.

Umbrella sampling simulations were carried out by applying a total of 49 harmonic umbrella windows (positioned between -12 \AA and 12 \AA , with a force constant of 10 kcal/mol/ \AA^2) along a reaction coordinate normal to the membrane plane (z -axis). The system for each window was pre-equilibrated for a time of 200 ps before a production run of 1 ns. The data were analyzed by using WHAM to yield a converged PMF (see Figure S1 for its convergence for symmetrized and unsymmetrized WHAM computations), consistent with previous studies,³² and providing an US-PMF reference. Note that single z may not represent the “true” physical coordinate for ion permeation across the gA channel at high ionic concentrations that likely give rise to double occupancy as part of the permeation mechanism.³⁸ The

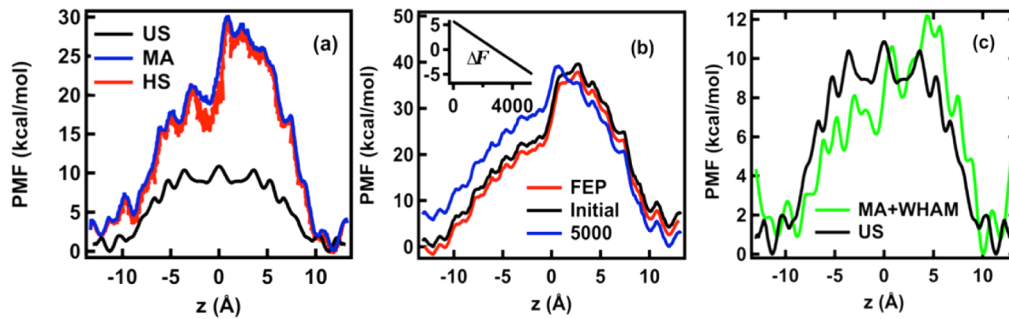


Figure 6. Potential of mean force (PMF) $G_0(z)$. (a) PMF (blue) computed by the MA estimator, quasi-harmonic approximation (red) proposed by Hummer and Szabo (HS), and US solved by using WHAM equations (black). (b) Free-energy profile computed by eq 1; the black curve is the PMF computed by eq 3 and the blue curve is the PMF after solving eqs 3 and 11 for 5000 iterations. Number of pulling frames n is only 15 in this convergence-test case. The inset shows the perturbed free-energy change $\Delta\mathcal{F} = \mathcal{F}(z_B) - \mathcal{F}(z_A)$ versus iteration steps. (c) PMFs computed by the MA+WHAM and US+WHAM equations. We used $n = 144$ forward and $n = 144$ backward pulling trajectories at $v = 100 \text{ \AA/ns}$, $\epsilon = 0.02 \text{ \AA}$ for panels a and c. One-nanosecond data in $49 \times 0.5 \text{ \AA}$ windows were collected in US.

simulations reported here offer a chance to compare performance of two methods (US and MA-estimator) for well-defined 1-dimensional reaction coordinates.

We used NAMD³⁹ for the pulling simulations¹⁰ with the same force field. First, we held the ion by using an applied harmonic potential $V_{f0} = k(z - z_A)^2/2$ at one end of gA and by using $V_{r0} = k(z - z_B)^2/2$ at the other end of the gA channel, where $k = 100 \text{ kcal/mol/\AA}^2$, $z_A = -13 \text{ \AA}$, and $z_B = 13 \text{ \AA}$. To define the pulling direction well, we applied a lateral constraint to the ion; that is, $V_L = k_L[(x - x_0)^2 + (y - y_0)^2]/2$ with $k_L = 0.1 \text{ kcal/mol/\AA}^2$, to enforce the pulling direction along the z -direction. This constraint is expected to introduce a certain bias to the computed PMFs. The expected bias can be estimated as $\frac{k_L R^2}{2} \approx 0.45 \text{ kcal/mol}$, where $R \approx 3 \text{ \AA}$ is the radius of the inner gA pore. An additional constraint was acting on the center of mass of the lipid bilayer to prevent bilayer drifting during relatively fast pulling simulations. A similar constraining scheme was used in a number of ion permeation and solute partitioning simulations in the past.^{31,40–42} As shown below, the constraints do not significantly affect the resulting PMFs in comparison with the PMFs from umbrella sampling.

We minimized the system for 5000 steps and equilibrated for 8–20 ns at $T = 310 \text{ K}$, $P = 1 \text{ atm}$ using a time step of 1 fs, Langevin dynamics for maintaining temperature, and Nosé–Hoover Langevin piston pressure control. The Particle Mesh Ewald method was also used for computing electrostatic interactions. Every 20 ps, we collected a configuration characterized by all of the instant coordinates and velocities for steered molecular dynamics simulations with pulling speeds $v = 100$ and 10 \AA/ns . For this system, we used $z_A = -13$ and $z_B = 13 \text{ \AA}$. Because the gA is a symmetric channel, we symmetrized the pulling data by reassigning

$$M(i) = [M(i) + M(Q - i)]/2 = M(Q - i)$$

which was used in computing PMFs³² via the US⁴³ and WHAM methods.^{20,44} We solved the WHAM equations for the pulling data with a convergence tolerance equal to 10^{-7} kcal/mol of PMFs.

2.1. Self-Consistency Algorithm: MA Estimator vs MA+WHAM Equations. Figure 6a shows that the PMF $G_0(z)$ computed by eq 3 (MA-PMF) maintains significant bias compared to the US-PMF. We also found that the quasi-harmonic approximation proposed by Hummer and Szabo¹⁷ returns a $G_0(z)$ that is similar to but noisier than the MA-PMF.

Those PMFs for $|z| < 10 \text{ \AA}$ are approximately 5–20 kcal/mol higher than the US-PMF. This provides clear evidence that the MA estimator can fail for computing $G_0(z)$ from a finite number of pulling trajectories with a fast pulling speed of 100 \AA/ns , although the estimator was found to be efficient in simple systems.^{16,17} This illustrates the point discussed in the introduction that a finite number of pulling trajectories generated in nonequilibrium simulations cannot guarantee the convergence of work distribution functions; thus, the MA estimator and quasi-harmonic approximation can fail. To tackle this possible failure, Minh and Adib also suggested solving eq 3 with

$$\exp[-\beta\Delta\mathcal{F}(s_f)] = \frac{\int dz e^{-\beta[G_0(z) + V_f(z; t)]}}{\int dz e^{-\beta[G_0(z) + V_f(z; 0)]}} \quad (11)$$

in a way similar to the WHAM equations. However, we found that the iteration scheme does not return a convergent $G_0(z)$. Figure 6b shows that the details of the PMF $G_0(z)$ after 5000 iterations (blue curve) are unchanged with respect to the initial PMF but appear to only be shifted. The PMF is shifted in a way such that the perturbed free-energy change $\Delta\mathcal{F} = \mathcal{F}_B - \mathcal{F}_A$ (shown in the inset) linearly increases with the iteration step, indicating that the PMF is divergent. This observation can be explained as follows: for such a strong harmonic potential ($k = 100 \text{ kcal/mol/\AA}^2$), eqs 3 and 11 can be approximately rewritten as

$$G_0(s_f) = \begin{cases} \Delta\mathcal{F}(s_f) + \delta_1 & \text{if } s_f > z_c \\ \Delta\mathcal{F}(s_f) + \delta_2 & \text{if } s_f < z_c \end{cases} \quad (12a)$$

$$\Delta\mathcal{F}(s_f) = G_0(s_f) - G_0(z_A) \quad (12b)$$

where δ_1 and δ_2 are constants and z_c is the position at which $W_f(z)$ crosses $W_r(z)$. For $s_f > z_c$, $\Delta\mathcal{F}(s_f)$ is strongly dependent on the backward-pulling data, while for $s_f < z_c$, $\Delta\mathcal{F}(s_f)$ is strongly dependent on the forward-pulling data. While this approximation can be readily understood when pulling speeds are very small, even in our case, with $v = 100 \text{ \AA/ns}$ or 10 \AA/ns , the differences between $\Delta\mathcal{F}(s_f)$ (free-energy profiles) and $G_0(s_f)$ (PMF) are also a constant (see the black and red curves in Figure 6b). By solving the approximated coupled equations, at every step, $\Delta\mathcal{F}(s_f)$ and $G_0(s_f)$ are changed by $\delta_1 - G_0(z_A)$ for $s_f > z_c$ or by $G_0(z_A) + \delta_2$ for $s_f < z_c$. These changes are shown in Figure 6b. The data collected in Figure 6b show that $\Delta\mathcal{F}$ linearly changes with the iteration step. This result suggests that in general cases, the

iteration scheme is unable to further remove bias in the nonequilibrium data and the coupled eqs 3 and 11 fail to yield convergence.

We found that by grouping the pulling data in windows represented by $M(i)$ and solving the WHAM eqs 5 and 6, the barriers in the MA-PMF can be significantly reduced (see Figure 6c). The unsymmetrized MA+WHAM PMF $G_0(z)$ has many features similar to the US PMF, such as (1) the overall barrier of 10–12 kcal/mol compared to that of 10–11 kcal/mol of the US PMF, (2) the similar relative free-energy minima and maxima, and (3) the close positions of the optima; however, the free-energy well seen from $|z| = 13 \text{ \AA}$ is different than that of the US-PMF (we will identify what causes the difference). Note that the pulling speed $v = 100 \text{ \AA/ns}$ is considered as very fast not only in the experiments but also in many reported pulling simulations, for example, in refs 11–13, which noted that the nonequilibrium statistics using Jarzynski's Equality and Crooks' theorem were not as efficient and reliable for estimating nonbiased PMFs for a finite number of pulling simulations as the commonly used umbrella sampling and WHAM methods. However, the results in this paper will further show that the combination of the MA estimator and WHAM equations is remarkably efficient at reducing bias in nonequilibrium data. From now on, we will symmetrize the data (see Methodology) to enhance the statistics. The following sections will address the issues and effects of parameters such as bin width and binning regions of collected data (see section S2 in the Supporting Information), force constants, pulling speeds, and number of trajectories on the accuracy and convergence of the MA+WHAM PMFs $G_0(z)$.

2.2. Effects of Force Constant. Figure 7a shows that both the nonequilibrium estimators and our proposed method fail to

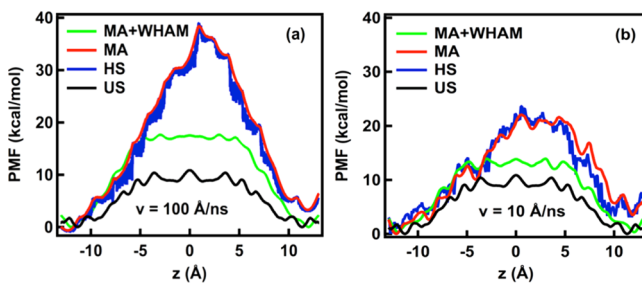


Figure 7. Potential of mean force (PMF) $G_0(z)$ at $k = 10 \text{ kcal/mol/}\text{\AA}^2$ and $\epsilon = 0.1 \text{ \AA}$: (a) 144 forward and 144 backward trajectories and $v = 100 \text{ \AA/ns}$; (b) 2 forward and 2 backward trajectories and $v = 10 \text{ \AA/ns}$.

produce accurate PMFs when the force constant $k = 10 \text{ kcal/mol/}\text{\AA}^2$ and $v = 100 \text{ \AA/ns}$. However, when $v = 10 \text{ \AA/ns}$, the overall barriers of all the PMFs in Figure 7b are significantly reduced in comparison with those in Figure 7a, even when using $n = 2$ trajectories. Another noticeable feature is that the MA-PMF for $k = 10 \text{ kcal/mol/}\text{\AA}^2$ (Figure 7a) has a peak of 15 kcal/mol higher than the one for $k = 100 \text{ kcal/mol/}\text{\AA}^2$ found in Figure 6a. These results suggest that both smaller pulling speeds and stronger values of k can significantly reduce bias in the MA-PMFs. The reason is that stronger k makes the approximation of the delta-Dirac function more accurate for the binning histogram construction, thus more accurate PMFs. But smaller values of k may not hold a reaction coordinate strongly enough with respect to the corresponding steering point near transition states, particularly at very fast pulling speeds, thus incurring larger dissipated work, at which the less accurate approximation of the delta-Dirac function may not return reliable histograms for the

WHAM equations. Therefore, the resulting values of work can be easily biased, as observed in the MA-PMFs. Furthermore, even when solving the WHAM equations for these pulling data, the overall barrier of the MA+WHAM PMFs might be the same as in the case of $k = 100 \text{ kcal/mol/}\text{\AA}^2$, but the details of the relative free-energy optima for $v = 100 \text{ \AA/ns}$ and $k = 10 \text{ kcal/mol/}\text{\AA}^2$ appear to be invisible (see Figure 7a).

2.3. Effects of the Number of Trajectories at Different Pulling Speeds. An important conclusion of this paper is that the MA+WHAM estimator can return reliable PMFs with just a few pulling trajectories. Figure 8a shows the PMFs at $v = 100 \text{ \AA/ns}$,

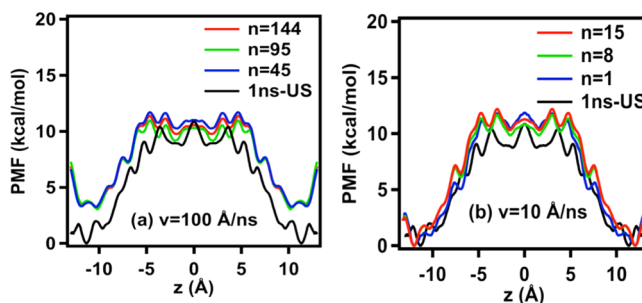


Figure 8. Potential of mean force (PMF) $G_0(z)$ at different numbers of pulling trajectories. (a) Discard data outside of $[z_A:z_B]$, $\epsilon = 0.02 \text{ \AA}$, and uncertainty $\sigma_{\text{WHAM}} = 0.33 \text{ kcal/mol}$ for $n = 144$. The simulation time for the 144 trajectories in one direction is 37.44 ns. (b) Use all pulling data, $\epsilon = 0.1 \text{ \AA}$, and uncertainty $\sigma_{\text{WHAM}} = 2.3 \text{ kcal/mol}$ for $n = 15$. The simulation time for the 15 trajectories in one direction is 39 ns.

whose data outside $[z_A:z_B]$ at $\epsilon = 0.02 \text{ \AA}$ at the fastest pulling speed are discarded for three sets of forward–backward pulling trajectories. Although the resulting PMFs are not accurate given a finite number of trajectories (see section S2), they look more comparable to the US-PMF even at $n = 45$ than the PMFs¹¹ computed from much slower (2.5 – 10 \AA/ns) pulling simulations via Jarzynski's Equality. Figure 8b shows that the PMFs at $v = 10 \text{ \AA/ns}$, which are computed with all possible data (see section S2) from 15 forward–backward pulling trajectories, are very close to the US-PMF in terms of the first free-energy well, overall and relative free-energy barriers, with differences of 1–2.0 kcal/mol. The computational cost of the 15 forward–backward pulling trajectories are equivalent to that of the 144 trajectories at $v = 100 \text{ \AA/ns}$. This clearly indicates that the PMFs from slower pulling simulations should be more accurate than the faster pulling simulations given the same computational cost. Section 1 also suggested that simulations with fast pulling speeds might end up having so many pulling trajectories with little improvement in the accuracy of the resulting PMFs.

Figure 8b also shows that the PMFs computed from fewer trajectories are not much different from the PMFs with 4–15 times more trajectories, although σ_{WHAM} obtained from fewer trajectories are larger by a few kcal/mol. For example, σ_{WHAM} for the PMF with one forward–backward pulling trajectory is approximately 8 kcal/mol, which is four times larger than σ_{WHAM} for $n = 15$. Another point is that on the one hand, σ_{WHAM} for the PMFs at $v = 100 \text{ \AA/ns}$ shown in Figure 8a is only 0.33 kcal/mol, which is smaller than the uncertainty of 2.3 kcal/mol for the PMFs at $v = 10 \text{ \AA/ns}$ (Figure 8b). On the other hand, the PMFs at $v = 10 \text{ \AA/ns}$ appear to be much less biased than the ones at $v = 100 \text{ \AA/ns}$ (Figure 8). Regarding computational costs, the faster pulling simulations ($v = 100 \text{ \AA/ns}$) with $n = 45$ forward and $n = 45$ backward trajectories require 23.4 ns, while the slower pulling

simulations ($v = 10 \text{ \AA/ns}$) with $n = 1$ forward and $n = 1$ backward trajectories require only 5.2 ns. This suggests that simulations of many fast-pulling trajectories are not as reliable and efficient as simulations of few slower pulling trajectories for computing PMFs, and that σ_{WHAM} is not always a trusted measure of uncertainty but the test of different sets of pulling trajectories at different pulling speeds.

REMARKS AND CONCLUSIONS

We report an advance in computing convergent and unbiased PMFs $G_0(z)$ for a one-dimensional model system and a gA channel from pulling simulations. The gA system posed a challenge for recovering $G_0(z)$ via Jarzynski's equality at pulling speeds of $2.5\text{--}10 \text{ \AA/ns}$.¹¹ We show that even in the cases where our pulling speeds are from 10 and 100 \AA/ns , the proposed method is able to recover the details of major free-energy barriers and minima of an ion traversing the gA channel. The simulation time scales of 5–25 ns can be used to generate pulling trajectories for postprocessing PMFs that are, for the first time, comparable with the results obtained from 0.1 to 0.3 ns/window umbrella sampling simulations of 50 windows (see S1 in *Supporting Information*). To our knowledge, none of the previous studies on nonequilibrium sampling^{11,19} were able to reconstruct $G_0(z)$ as close to the US PMF as our PMFs at a pulling speed of 10 \AA/ns and a simulation time of 10 ns.

The successful use of the WHAM algorithm for forward and backward pulling trajectories, with initial estimates of PMFs obtained from the MA estimator, suggests that the WHAM equations minimizing biases could potentially be extended to retrieve equilibrium PMFs from nonequilibrium sampling in a more complex setting. This also implies that the use of nonequilibrium estimators alone may not be always reliable for computing PMFs; particularly, in systems with complex reaction coordinates such as the gA channel, and given a small number of pulling trajectories, the forward and backward work distribution functions do not cross each other. It is important to note that the histogram-building procedures used to approximate the Dirac delta function have relatively minor effect on the quality of PMF estimates. Figure S3 shows that the reduction of bin width ϵ in the histogram procedure, which presumably results in better approximation of the Dirac delta function in eq 3, does not affect the PMF convergence. The histogram-building procedure combines, into a specific window, all possible values of biasing external potentials, which are sampled by not only dynamical values of a reaction coordinate but also slightly different steering points. This is an interesting observation because it connects directly to the original concept of the US method first used by Torrie and Valleau in 1977.⁴³ The purpose of the US is to sample a distribution of biasing external potentials, which must contain an unbiased probability distribution of a phase space independent of initial states. Roux^{22,44} showed that one can use a harmonic potential, which couples a reaction coordinate with its predefined values, and let dynamics sample all possible values of the reaction coordinate along a pathway, thus yielding a series of Boltzmann distributions of biasing external potentials. Therefore, if the WHAM equations are applicable to US data, they should also be so to pulling data (see *Methodology*). Of course, the effect of the quality of data on PMFs can be observed at different quantifiers (number of windows and equilibration times versus pulling speeds and number of forward and backward trajectories) for both US and pulling simulations, but conceptually, there should be no preference of sampled data if

the resulting distributions of biasing external potentials from both simulations are Boltzmann.

However, the use of the WHAM equations without the MA estimator was previously shown not to reproduce highly accurate PMFs¹⁹ for pulling trajectories along only one direction. The failure of the WHAM equations in the usage was attributed to the nonzero irreversible work, which was not properly removed in the nonequilibrium pulling data; so the formulation of the WHAM equations based on the equilibrium assumption would not hold. Our results suggest that using the MA estimator by means of Crooks' theorem can remove the nonzero irreversible work by appropriately weighing forward and backward pulling trajectories.

We also showed that the quality of pulling data with slower speeds and stronger force constants is better than data with faster speeds and softer force constants, given the same amount of simulation times. This is useful practically because one should avoid using very fast pulling speeds with a large number of trajectories. For example, in the model system (section 1), the pulling speeds can be as large as 15 \AA/ps to estimate PMFs with less than a 10% difference from the exact one, while in the gA system (Section 22), they should be as small as 10 \AA/ns . This is due to the fact that some transitions between two states can involve much more configuration sampling than others, thus requiring slow pulling rates for sufficiently exploring important intermediate states in a finite number of pulling trajectories. This suggests that one should choose pulling speeds not much larger than experimentally observed transition movements of reaction coordinates.

The use of the WHAM equations helps deliver a claim that a relatively small number of relatively fast pulling trajectories can be sufficient for reconstructing entire PMFs; thus, the applicability of efficient pulling simulations can be extended in systems with large dimensional phase space and high complexity of energetic landscapes. For example, it is possible to implement the pulling simulations in the scheme of string methods,^{45–48} which have been used to drive a complex protein system between the two end-point states along a minimum free-energy pathways. This technique presented in this study may allow for more accurate estimates of minimum free-energy pathways, and representing the state transitions in terms of velocity (or pulling speeds) fields in large dimensional spaces. We believe this method will also promote the use of the nonequilibrium sampling technique on a number of biophysical and biochemical problems in ion channels, transporters, and other proteins. It might be particularly more useful than US in the channel systems, in which nonequilibrium vs equilibrium permeation⁴⁹ and energetic pathways are of interest, whereas the US method usually returns equilibrium permeation and energetic pathways.

ASSOCIATED CONTENT

S Supporting Information

The Supporting Information is available free of charge on the ACS Publications website at DOI: [10.1021/acs.jctc.5b01050](https://doi.org/10.1021/acs.jctc.5b01050).

Convergence test for the potential of mean forces obtained from Umbrella Sampling simulations (PDF)

AUTHOR INFORMATION

Corresponding Author

*E-mail: snoskov@ucalgary.ca.

Author Contributions

▀ V.A.N. and I.K. contributed equally to this work. Please send an email to ngov@ucalgary.ca and nvan@usc.edu to request a Fortran code. Please send an email to ilsookim@usc.edu to request the python implementation of the MA estimator used in the benchmark.

Funding

This work in Calgary was supported by the Natural Sciences and Engineering Research Council of Canada (NSERC) (Discovery Grant RGPIN-315019 to SYN) and the Alberta Innovates Technology Futures (AITF) Strategic Chair in BioMolecular Simulations (Centre for Molecular Simulation). SYN is a Canadian Institute for Health Research New Investigator and an Alberta Innovates Health Solutions (AIHS) Scholar. VN is supported by AIHS Postdoctoral Fellowship.

Notes

The authors declare no competing financial interest.

ACKNOWLEDGMENTS

We acknowledge discussions and comments from Drs. David Sivak, Robert Farley, Christopher Jarzynski, David Minh, and Benoît Roux.

REFERENCES

- (1) Jarzynski, C. Nonequilibrium Equality for Free Energy Differences. *Phys. Rev. Lett.* **1997**, *78*, 2690–2693.
- (2) Jarzynska, C. Nonequilibrium Work Relations: Foundations and Applications. *Eur. Phys. J. B* **2008**, *64*, 331–340.
- (3) Crooks, G. Nonequilibrium Measurements of Free Energy Differences for Microscopically Reversible Markovian Systems. *J. Stat. Phys.* **1998**, *90*, 1481–1487.
- (4) Crooks, G. E. Entropy Production Fluctuation Theorem and the Nonequilibrium Work Relation for Free Energy Differences. *Phys. Rev. E: Stat. Phys., Plasmas, Fluids, Relat. Interdiscip. Top.* **1999**, *60*, 2721–2726.
- (5) Campisi, M.; Talkner, P.; Hanggi, P. Fluctuation Theorem for Arbitrary Open Quantum Systems. *Phys. Rev. Lett.* **2009**, *102*, 210401.
- (6) Andrieux, D.; Gaspard, P. Quantum Work Relations and Response Theory. *Phys. Rev. Lett.* **2008**, *100*, 230404.
- (7) Raman, S.; Utzig, T.; Baimpos, T.; Shrestha, B. R.; Valtiner, M. Deciphering the Scaling of Single-Molecule Interactions Using Jarzynski's Equality. *Nat. Commun.* **2014**, *5*, 5539.
- (8) Liphardt, J. T.; Dumont, S.; Smith, S. B.; Tinoco, I.; Bustamante, C. Experimental Test of Jarzynski's Equality: Recovering Equilibrium Information from Nonequilibrium Measurements. *Biophys. J.* **2002**, *82*, 193A–194A.
- (9) Collin, D.; Ritort, F.; Jarzynski, C.; Smith, S. B.; Tinoco, I., Jr.; Bustamante, C. Verification of the Crooks Fluctuation Theorem and Recovery of RNA Folding Free Energies. *Nature* **2005**, *437*, 231–4.
- (10) Park, S.; Khalili-Araghi, F.; Tajkhorshid, E.; Schulten, K. Free Energy Calculation from Steered Molecular Dynamics Simulations Using Jarzynski's Equality. *J. Chem. Phys.* **2003**, *119*, 3559–3566.
- (11) Baştug, T.; Kuyucak, S. Application of Jarzynski's Equality in Simple Versus Complex Systems. *Chem. Phys. Lett.* **2007**, *436*, 383–387.
- (12) Oberhofer, H.; Dellago, C.; Geissler, P. L. Biased Sampling of Nonequilibrium Trajectories: Can Fast Switching Simulations Outperform Conventional Free Energy Calculation Methods? *J. Phys. Chem. B* **2005**, *109*, 6902–15.
- (13) Rodriguez-Gomez, D.; Darve, E.; Pohorille, A. Assessing the Efficiency of Free Energy Calculation Methods. *J. Chem. Phys.* **2004**, *120*, 3563–78.
- (14) Kofke, D. A. On the Sampling Requirements for Exponential-Work Free-Energy Calculations. *Mol. Phys.* **2006**, *104*, 3701–3708.
- (15) Jarzynski, C. Rare Events and the Convergence of Exponentially Averaged Work Values. *Phys. Rev. E* **2006**, *73*, 046105 DOI: [10.1103/PhysRevE.73.046105](https://doi.org/10.1103/PhysRevE.73.046105).
- (16) Minh, D. D. L.; Adib, A. B. Optimized Free Energies from Bidirectional Single-Molecule Force Spectroscopy. *Phys. Rev. Lett.* **2008**, *100*, 180602.
- (17) Hummer, G.; Szabo, A. Free Energy Profiles from Single-Molecule Pulling Experiments. *Proc. Natl. Acad. Sci. U. S. A.* **2010**, *107*, 21441–21446.
- (18) Ngo, V. A.; Haas, S. Demonstration of Jarzynski's Equality in Open Quantum Systems Using a Stepwise Pulling Protocol. *Phys. Rev. E Stat. Nonlin. Soft Matter Phys.* **2012**, *86*, 031127.
- (19) Gullingsrud, J. R.; Braun, R.; Schulten, K. Reconstructing Potentials of Mean Force through Time Series Analysis of Steered Molecular Dynamics Simulations. *J. Comput. Phys.* **1999**, *151*, 190–211.
- (20) Kumar, S.; Rosenberg, J. M.; Bouzida, D.; Swendsen, R. H.; Kollman, P. A. The Weighted Histogram Analysis Method for Free-Energy Calculations on Biomolecules. I. The Method. *J. Comput. Chem.* **1992**, *13*, 1011–1021.
- (21) Zhu, F.; Hummer, G. Convergence and Error Estimation in Free Energy Calculations Using the Weighted Histogram Analysis Method. *J. Comput. Chem.* **2012**, *33*, 453–65.
- (22) Souaille, M.; Roux, B. Extension to the Weighted Histogram Analysis Method: Combining Umbrella Sampling with Free Energy Calculations. *Comput. Phys. Commun.* **2001**, *135*, 40–57.
- (23) Minh, D. D. Multidimensional Potentials of Mean Force from Biased Experiments Along a Single Coordinate. *J. Phys. Chem. B* **2007**, *111*, 4137–40.
- (24) Bennett, C. H. Efficient Estimation of Free-Energy Differences from Monte-Carlo Data. *J. Comput. Phys.* **1976**, *22*, 245–268.
- (25) Hummer, G.; Szabo, A. Free Energy Reconstruction from Nonequilibrium Single-Molecule Pulling Experiments. *Proc. Natl. Acad. Sci. U. S. A.* **2001**, *98*, 3658–3661.
- (26) Kim, I.; Allen, T. W. Bennett's Acceptance Ratio and Histogram Analysis Methods Enhanced by Umbrella Sampling Along a Reaction Coordinate in Configurational Space. *J. Chem. Phys.* **2012**, *136*, 164103.
- (27) Hummer, G.; Szabo, A. Calculation of Free-Energy Differences from Computer Simulations of Initial and Final States. *J. Chem. Phys.* **1996**, *105*, 2004–2010.
- (28) Kim, I.; Warshel, A. A Microscopic Capacitor Model of Voltage Coupling in Membrane Proteins: Gating Charge Fluctuations in Ci-Vsd. *J. Phys. Chem. B* **2016**, DOI: [10.1021/acs.jpcb.5b10956](https://doi.org/10.1021/acs.jpcb.5b10956).
- (29) Ketcham, R. R.; Hu, W.; Cross, T. A. High-Resolution Conformation of Gramicidin A in a Lipid Bilayer by Solid-State Nmr. *Science* **1993**, *261*, 1457–60.
- (30) Allen, T. W.; Andersen, O. S.; Roux, B. Structure of Gramicidin A in a Lipid Bilayer Environment Determined Using Molecular Dynamics Simulations and Solid-State Nmr Data. *J. Am. Chem. Soc.* **2003**, *125*, 9868–9877.
- (31) Allen, T. W.; Andersen, O. S.; Roux, B. Energetics of Ion Conduction through the Gramicidin Channel. *Proc. Natl. Acad. Sci. U. S. A.* **2004**, *101*, 117–122.
- (32) Allen, T. W.; Andersen, O. S.; Roux, B. Molecular Dynamics - Potential of Mean Force Calculations as a Tool for Understanding Ion Permeation and Selectivity in Narrow Channels. *Biophys. Chem.* **2006**, *124*, 251–67.
- (33) Allen, T. W.; Andersen, O. S.; Roux, B. Ion Permeation through a Narrow Channel: Using Gramicidin to Ascertain All-Atom Molecular Dynamics Potential of Mean Force Methodology and Biomolecular Force Fields. *Biophys. J.* **2006**, *90*, 3447–3468.
- (34) Busath, D. D.; et al. Noncontact Dipole Effects on Channel Permeation. I. Experiments with (Sf-Indole)Trp13 Gramicidin A Channels. *Biophys. J.* **1998**, *75*, 2830–44.
- (35) MacKerell, A. D.; et al. All-Atom Empirical Potential for Molecular Modeling and Dynamics Studies of Proteins. *J. Phys. Chem. B* **1998**, *102*, 3586–616.
- (36) Beglov, D.; Roux, B. Finite Representation of an Infinite Bulk System: Solvent Boundary Potential for Computer Simulations. *J. Chem. Phys.* **1994**, *100*, 9050–9063.
- (37) Jorgensen, W. L.; Chandrasekhar, J.; Madura, J. D.; Impey, R. W.; Klein, M. L. Comparison of Simple Potential Functions for Simulating Liquid Water. *J. Chem. Phys.* **1983**, *79*, 926–935.

- (38) Li, Y. H.; Andersen, O. S.; Roux, B. Energetics of Double-Ion Occupancy in the Gramicidin a Channel. *J. Phys. Chem. B* **2010**, *114*, 13881–13888.
- (39) Phillips, J. C.; Braun, R.; Wang, W.; Gumbart, J.; Tajkhorshid, E.; Villa, E.; Chipot, C.; Skeel, R. D.; Kale, L.; Schulten, K. Scalable Molecular Dynamics with Namd. *J. Comput. Chem.* **2005**, *26*, 1781–802.
- (40) Vorobyov, I.; Bennett, W. F. D.; Tielemans, D. P.; Allen, T. W.; Noskov, S. The Role of Atomic Polarization in the Thermodynamics of Chloroform Partitioning to Lipid Bilayers. *J. Chem. Theory Comput.* **2012**, *8*, 618–628.
- (41) Vorobyov, I.; Li, L. B.; Allen, T. W. Assessing Atomistic and Coarse-Grained Force Fields for Protein-Lipid Interactions: The Formidable Challenge of an Ionizable Side Chain in a Membrane. *J. Phys. Chem. B* **2008**, *112*, 9588–9602.
- (42) Allen, T. W.; Andersen, O.; Roux, B. Energetics of Ion Conduction through the Gramicidin Channel. *Proc. Natl. Acad. Sci. U. S. A.* **2004**, *86*, 351A–351A.
- (43) Torrie, G. M.; Valleau, J. P. Nonphysical Sampling Distributions in Monte Carlo Free-Energy Estimation: Umbrella Sampling. *J. Comput. Phys.* **1977**, *23*, 187–199.
- (44) Roux, B. The Calculation of the Potential of Mean Force Using Computer-Simulations. *Comput. Phys. Commun.* **1995**, *91*, 275–282.
- (45) Ren, W.; Vanden-Eijnden, E.; Maragakis, P.; E, W. N. Transition Pathways in Complex Systems: Application of the Finite-Temperature String Method to the Alanine Dipeptide. *J. Chem. Phys.* **2005**, *123*, 134109.
- (46) E, W.; Ren, W. Q.; Vanden-Eijnden, E. Finite Temperature String Method for the Study of Rare Events. *J. Phys. Chem. B* **2005**, *109*, 6688–6693.
- (47) E, W.; Ren, W. Q.; Vanden-Eijnden, E. String Method for the Study of Rare Events. *Phys. Rev. B: Condens. Matter Mater. Phys.* **2002**, *66*, 052301 DOI: [10.1103/PhysRevB.66.052301](https://doi.org/10.1103/PhysRevB.66.052301).
- (48) Pan, A. C.; Sezer, D.; Roux, B. Finding Transition Pathways Using the String Method with Swarms of Trajectories. *J. Phys. Chem. B* **2008**, *112*, 3432–3440.
- (49) Ngo, V.; Wang, Y.; Haas, S.; Noskov, S. Y.; Farley, R. A. K+ Block Is the Mechanism of Functional Asymmetry in Bacterial Nav Channels. *PLoS Comput. Biol.* **2016**, *12*, e1004482.